A novel requirement for ubiquitin-conjugating enzyme UBC-13 in retrograde recycling of MIG-14/Wntless and Wnt signaling

Junbing Zhang[a,b,c], Jinchao Liu[c], Anne Norris[d], Barth D. Grant[d], and Xiaochen Wang[c,e,*]
[a]College of Life Science, Beijing Normal University, Beijing 100875, China; [b]National Institute of Biological Sciences, Beijing 102206, China; [c]National Laboratory of Biomacromolecules, CAS Center for Excellence in Biomacromolecules, Institute of Biophysics, Chinese Academy of Sciences, Beijing 100101, China; [d]Department of Molecular Biology and Biochemistry, Rutgers University, Piscataway, NJ 08854; [e]College of Life Sciences, University of Chinese Academy of Sciences, Beijing 100049, China

ABSTRACT **After endocytosis, transmembrane cargoes such as signaling receptors, channels, and transporters enter endosomes where they are sorted to different destinations. Retromer and ESCRT (endosomal sorting complex required for transport) are functionally distinct protein complexes on endosomes that direct cargo sorting into the recycling retrograde transport pathway and the degradative multivesicular endosome pathway (MVE), respectively. Cargoes destined for degradation in lysosomes are decorated with K63-linked ubiquitin chains, which serve as an efficient sorting signal for entry into the MVE pathway. Defects in K63-linked ubiquitination disrupt MVE sorting and degradation of membrane proteins. Here, we unexpectedly found that UBC-13, the E2 ubiquitin-conjugating enzyme that generates K63-linked ubiquitin chains, is essential for retrograde transport of multiple retromer-dependent cargoes including MIG-14/Wntless. Loss of *ubc-13* disrupts MIG-14/Wntless trafficking from endosomes to the Golgi, causing missorting of MIG-14 to lysosomes and impairment of Wnt-dependent processes. We observed that retromer-associated SNX-1 and the ESCRT-0 subunit HGRS-1/Hrs localized to distinct regions on a common endosome in wild type but overlapped on *ubc-13(lf)* endosomes, indicating that UBC-13 is important for the separation of retromer and ESCRT microdomains on endosomes. Our data suggest that cargo ubiquitination mediated by UBC-13 plays an important role in maintaining the functionally distinct subdomains to ensure efficient cargo segregation on endosomes.**

Monitoring Editor
Adam Linstedt
Carnegie Mellon University

Received: Nov 13, 2017
Revised: Jun 8, 2018
Accepted: Jun 15, 2018

INTRODUCTION

The endocytic pathway regulates uptake, sorting, and the subsequent recycling and degradation of a variety of cargoes to maintain cellular polarity and homeostasis. After internalization, cargoes that enter into the pleiomorphic early endosomes are sorted to be recycled back to the plasma membrane, selected for inclusion in multivesicular bodies (MVBs) for lysosomal degradation, or delivered to the *trans*-Golgi network (TGN) through the retrograde transport pathway. These processes are controlled by coordinated actions of small GTPases, coat proteins, and protein complexes such as retromer and ESCRT (endosomal sorting complex required for transport).

Caenorhabditis elegans RAB-10 and its human homologue RAB10 are key regulators of endocytic recycling that deliver cargo back to plasma membranes through early endosomes and recycling endosomes (Babbey *et al.*, 2006; Chen *et al.*, 2006; Sano *et al.*, 2007). In the polarized *C. elegans* intestine, RAB-10 is required for the basolateral recycling of ectopically expressed human IL-2 receptor alpha-chain TAC (hTAC) between early endosomes and recycling endosomes (Chen *et al.*, 2006; Shi *et al.*, 2010, 2012).

This article was published online ahead of print in MBoC in Press (http://www.molbiolcell.org/cgi/doi/10.1091/mbc.E17-11-0639) on June 21, 2018.
The authors declare no competing financial interests.
*Address correspondence to: Xiaochen Wang (wangxiaochen@ibp.ac.cn).
Abbreviations used: ESCRT, endosomal sorting complex required for transport; GFP, enhanced green fluorescent protein; Hrs, hepatocyte-growth-factor–regulated tyrosine kinase substrate; hTAC, human IL-2 receptor alpha-chain; hTfR, human transferrin receptor; ILVs, intraluminal vesicles; MVBs, multivesicular bodies; MVE, multivesicular endosome pathway; STAM, signal transducing adaptor molecule; TGN, *trans*-Golgi network.

The sorting of transmembrane cargoes into the recycling retrograde transport pathway or the degradative multivesicular endosomal pathway (MVE) is mainly controlled by retromer and ESCRT, two functionally distinct protein complexes on endosomes. Retromer and ESCRT coexist on endosomes, but the molecular mechanisms that regulate their opposing activity and coordinate the cargo sorting process are not well understood. Retromer is an evolutionarily conserved multimeric complex consisting of a cargo-selective trimer Vps26-Vps29-Vps35 and a sorting nexin (SNX-BAR) dimer (Bonifacino and Hurley, 2008; Seaman, 2012; Burd and Cullen, 2014). The cargo-selective complex recognizes most known cargo proteins, while the SNX-BAR subunits induce the formation of high-curvature membrane transport tubules on endosomes that carry the cargoes (Carlton *et al.*, 2004; Bonifacino and Hurley, 2008; Burd and Cullen, 2014). The SNX subunits were recently shown to also have some intrinsic cargo sorting capacity, and to mediate the recycling of CI-MPR independently of the Vps26-Vps29-Vps35 trimer (Kvainickas *et al.*, 2017; Simonetti *et al.*, 2017). Many retromer-dependent cargoes have been identified including the Wnt transport protein Wntless/MIG-14 (Banziger *et al.*, 2006; Bartscherer *et al.*, 2006; Goodman *et al.*, 2006; Belenkaya *et al.*, 2008; Franch-Marro *et al.*, 2008; Pan *et al.*, 2008; Port *et al.*, 2008; Yang *et al.*, 2008). In *C. elegans*, SNX-3, a sorting nexin that lacks a BAR domain, is important for retrieving MIG-14 from early endosomes and delivering it to the TGN, while loss of the PX-BAR domain-containing sorting nexin SNX-1 and its interacting DNAJ domain-containing protein RME-8 also impairs MIG-14 trafficking, leading to missorting of MIG-14 to lysosomes and defects in Wnt-mediated processes (Shi *et al.*, 2009; Harterink *et al.*, 2011). Thus, multiple mechanisms are engaged to ensure proper recycling of Wntless/MIG-14 from endosomes to the Golgi.

Cargoes that are destined for degradation are sorted on endosomes by the ESCRT machinery into MVBs that fuse with lysosomes, where cargoes are released and broken down. In this process, cargoes are tagged with a ubiquitin sorting signal, which is recognized initially by Hrs (hepatocyte-growth-factor–regulated tyrosine kinase substrate), an ESCRT-0 component (Raiborg and Stenmark, 2009; Henne *et al.*, 2011). The ubiquitinated cargoes captured by ESCRT-0 are then handed over sequentially to ESCRT-I and -II or recruited to the ESCRT-I-II supercomplex before being incorporated into intraluminal vesicles (ILVs) for delivery to lysosomes (Haglund and Dikic, 2012). Cargo ubiquitination, including monoubiquitination, multiple monoubiquitination, and K63-linked polyubiquitination, occurs at plasma membranes and early endosomes to trigger internalization and the subsequent sorting of cargoes to the degradative MVE pathway (Raiborg and Stenmark, 2009; Haglund and Dikic, 2012). K63-linked polyubiquitination can direct cargo endocytosis but acts more efficiently as the signal for ESCRT-dependent sorting to MVBs (Belgareh-Touze *et al.*, 2008; Lauwers *et al.*, 2010; Erpapazoglou *et al.*, 2012, 2014; Huang *et al.*, 2013). In addition to serving as the sorting tag, cargo ubiquitination is required for ILV formation, which suggests that ubiquitinated cargoes have active roles in the sorting process (MacDonald *et al.*, 2012).

Ubc13 is an E2 ubiquitin-conjugating enzyme that generates K63-linked ubiquitin chains involved in diverse cellular processes (Hodge *et al.*, 2016). Consistent with the role of K63-linked ubiquitination in cargo sorting to the degradative pathway, Ubc13 is found to be recruited by the virus protein K3 to mediate K63-linked polyubiquitination of MHC class I molecules, which is important for lysosomal degradation of the protein (Duncan *et al.*, 2006). Moreover, loss of UBC-13–dependent K63-linked ubiquitination in *C. elegans* blocks degradation of maternal membrane proteins, causing their recycling to the cell surface (Sato *et al.*, 2014).

In this study, we unexpectedly found that UBC-13 is essential for retrograde transport of retromer-dependent cargoes including MIG-14/Wntless from endosomes to the Golgi. Loss of *ubc-13* causes missorting of MIG-14 to lysosomes and impairs Wnt-dependent processes. Our data suggest that cargo ubiquitination mediated by UBC-13 is important for maintaining the functionally distinct microdomains on endosomes to ensure efficient cargo sorting into different pathways.

RESULTS

Loss of E2 ubiquitin-conjugating enzyme UBC-13 affects MIG-14 trafficking

The *C. elegans* Wntless/MIG-14 cycles between the plasma membrane, the endosome, and the Golgi through a retrograde transport pathway (Yang *et al.*, 2008; Shi *et al.*, 2009; Harterink *et al.*, 2011). In the wild-type intestine, MIG-14::GFP was observed on basolateral plasma membranes and in small punctate early endosomes and Golgi ministacks (Figures 1, A and B, and 2, A–A″ and D–D″, Supplemental Figure S2, A–A″). We found that in *tm3546*, a deletion mutation of *ubc-13*, which encodes an E2 ubiquitin-conjugating enzyme, MIG-14::GFP was highly abnormal (Figure 1, C and D, and Supplemental Figure S1A). In *ubc-13(tm3546)*, MIG-14::GFP accumulated in intracellular membranes as both punctate and ring-like structures and these phenotypes were rescued by expression of UBC-13, indicating that loss of *ubc-13* affects MIG-14/Wntless trafficking (Figure 1, C, D, M, and N, and Supplemental Figure S1, A–E). RNA interference (RNAi) inactivation of APS-2 (the sigma 2 subunit of the clathrin adaptor complex AP-2) blocks clathrin-mediated endocytosis (Gu *et al.*, 2013). After *aps-2 RNAi* in a *ubc-13* mutant, we observed significantly reduced accumulation of MIG-14::GFP fluorescence on internal membranes, and increased accumulation of MIG-14::GFP on the basolateral plasma membranes (Figure 1, I–L, M, and N; Pan *et al.*, 2008). This suggests that *ubc-13* mutant-associated MIG-14::GFP trafficking defects occur after AP-2–dependent endocytosis of MIG-14::GFP, and that UBC-13 normally regulates trafficking of MIG-14 at a step downstream from clathrin-mediated endocytosis. UBC-13 was widely expressed in multiple cell types including neuronal cells, intestine cells, and EGL-20/Wnt–producing cells (Supplemental Figure S1, F–K′). Expression of wild-type but not catalytically inactive UBC-13 rescued the MIG-14 trafficking defects (Supplemental Figure S1, B–D). Moreover, UBC-13 expression controlled by the intestine-specific promoter *vha-6* led to a full rescue of MIG-14 trafficking defects in the *ubc-13(lf)* intestine (Supplemental Figure S1, B and E). These data indicate that UBC-13 regulates MIG-14 trafficking in a cell-autonomous manner and this function requires the ubiquitin-conjugating activity of UBC-13. Consistent with this, loss of UEV-1, the noncatalytic E2 variant that associates with UBC-13 to mediate K63-linked polyubiquitination, caused similar MIG-14 trafficking defects as in *ubc-13(lf)* (Figure 1, E, F, M, and N).

MIG-14 is missorted to late endosomes and lysosomes in *ubc-13* mutants

In the wild-type intestine, MIG-14::GFP appeared on basolateral plasma membranes, early endosomes, and the Golgi apparatus, as judged by its colocalization with PLCδ1-PH, RME-8, and MANS, which label these membrane compartments respectively (Figure 2, A–A″, D–D″, and J, and Supplemental Figure S2, A–A″ and F). MIG-14::GFP was separated from CHERRY::RAB-7, indicating that it is absent from late endosomes and lysosomes (Figure 2, G–G″ and K). In *ubc-13(tm3546)*, however, MIG-14::GFP was absent from plasma membranes or MANS-positive puncta but appeared on the limiting membrane of RAB-7-positive vesicles (Figure 2, B–B″, E–E″, H–H″,

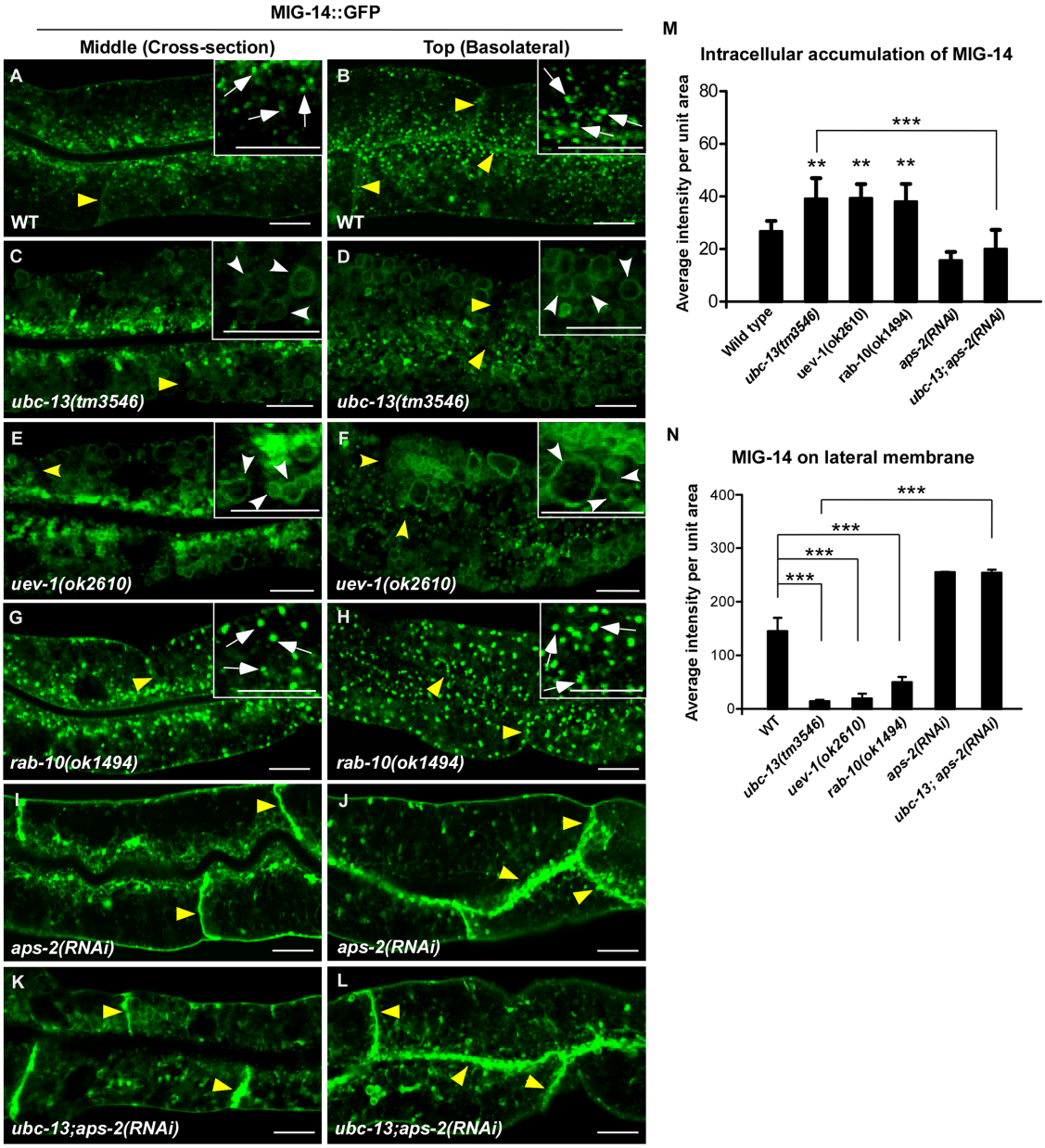

FIGURE 1: MIG-14 trafficking is affected in *ubc-13*, *uev-1*, and *rab-10* mutants. (A–L) Confocal fluorescence images of the intestine at the middle and the basolateral focal planes in wild type (WT; A, B), *ubc-13* (C, D), *uev-1* (E, F), *rab-10* (G, H), *aps-2(RNAi)* (I, J), and *ubc-13;aps-2(RNAi)* (K, L) expressing MIG-14::GFP. White arrows and arrowheads indicate MIG-14::GFP-labeled punctate and vesicular structures, respectively, in the cytosol of intestine cells. Yellow arrowheads indicate basal or lateral membranes of intestinal cells. (M, N) The average fluorescence intensity per unit area of MIG-14::GFP in the cytoplasm (M) and the lateral plasma membranes (N) of intestine cells was quantified in the indicated strains. At least eight animals were scored in each strain and data are shown as mean ± SD. One-way ANOVA with Tukey's post hoc test was performed to compare all the other data sets with wild type or data sets that are linked by lines. **, $P < 0.001$; ***, $P < 0.0001$. In A–L, scale bars indicate 10 μm.

J, and K). The colocalization of MIG-14 and RME-8 was unaffected in *ubc-13* mutants (Figure S2, B–B″ and F). Loss of MIG-14 from the Golgi, and its redistribution to late endosomes and lysosomes, suggest that loss of UBC-13 impairs MIG-14 retrograde recycling from endosomes to the Golgi.

UBC-13 and RAB-10 regulate MIG-14 trafficking through distinct pathways

RAB-10 is a key regulator of endocytic recycling in polarized epithelial cells like *C. elegans* intestinal cells. Loss of RAB-10 causes abnormally enlarged early endosomes and blocks basolateral recycling of hTAC through a retromer-independent, ARF-6–dependent, pathway (Chen *et al.*, 2006; Shi *et al.*, 2010, 2012). We found that MIG-14::GFP was present on RAB-10–positive vesicles, and loss of *rab-10* affected MIG-14 recycling, causing significantly reduced MIG-14::GFP on basolateral membranes and increased GFP fluorescence on intracellular membranes (Figures 1, G, H, M, and N, and 2, C–C″, and Supplemental Figure S2, D–D″ and G). The pattern of intracellular MIG-14 accumulation in *rab-10(lf)*, however, was different from that in *ubc-13* mutants. In *rab-10(ok1494)* mutants, the intracellularly

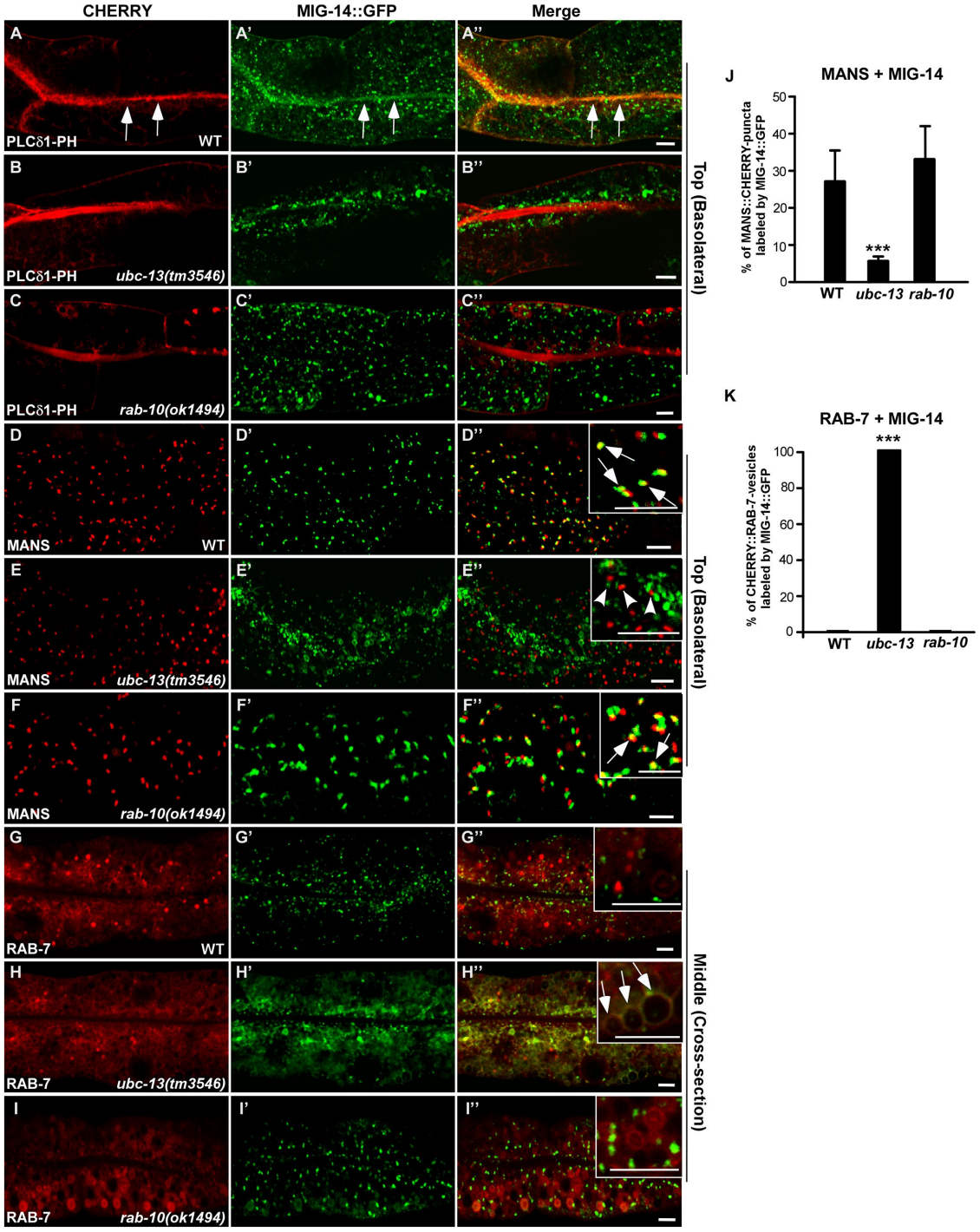

FIGURE 2: MIG-14 is missorted to late endosomes and lysosomes in *ubc-13(lf)* mutants. (A–I″) Confocal fluorescence images of the intestine at the middle and the basolateral focal plane in wild-type (WT; A–A″, D–D″, G–G″), *ubc-13(tm3546)* (B–B″, E–E″, H–H″), and *rab-10(ok1494)* (C–C″, F–F″, I–I″) animals coexpressing MIG-14::GFP and CHERRY::PLCδ1-PH (A–C″), MANS::CHERRY (D–F″), or CHERRY::RAB-7 (G–I″). Arrows indicate colocalization of GFP and CHERRY. Arrowheads indicate puncta that are labeled by MANS::CHERRY but not MIG-14::GFP. (J, K) Colocalization of MIG-14::GFP with MANS::CHERRY (J) or CHERRY::RAB-7 (K) in wild type, *ubc-13*, and *rab-10* was quantified. At least five animals were scored in each strain, and data are shown as mean ± SD. One-way ANOVA with Tukey's post hoc test was performed to compare all the other data sets with wild type. ***, $P < 0.0001$. All other points had $P > 0.05$. Scale bars: 5 μm.

accumulated MIG-14::GFP appeared on enlarged RME-8–positive early endosomes but was absent from RAB-7–positive late endosomes or lysosomes (Figure 2, I–I″ and K, and Supplemental Figure S2, C–C″ and F). Importantly, localization of MIG-14 to the Golgi was unaltered in *rab-10(ok1494)*, indicating that endosome-to-Golgi transport of MIG-14 was not affected (Figure 2, F–F″ and J). Taken together, these data suggest that RAB-10 promotes MIG-14 recycling from early endosomes to the plasma membrane, and loss of RAB-10 function caused accumulation of MIG-14 on abnormal early endosomes. Loss of RAB-10 did not cause redistribution of MIG-14

to late endosomes and lysosomes, in contrast to mutants defective in endosome-to-Golgi retrograde recycling.

MIG-14::GFP appeared mostly as ring-like structures in *ubc-13(tm3546)*, but accumulated as puncta in *rab-10(lf)* worms (Figure 3, A–D). MIG-14 puncta and MIG-14 rings were observed in double mutants defective in both *ubc-13* and *rab-10*, and the total intracellular GFP fluorescence intensity was significantly higher than in either of the single mutants (Figure 3, E–G). Collectively, these data suggest that RAB-10 and UBC-13 recycle MIG-14 through distinct pathways; RAB-10 recycles MIG-14 from early endosomes to the plasma membrane, while UBC-13 is required for retrograde transport of MIG-14 from endosomes to the Golgi.

Retrograde transport of MIG-14 is more severely affected when both UBC-13 and SNX-1 retromer complex are defective

The retromer complex is responsible for transporting MIG-14 from endosomes to the Golgi, and loss of retromer function leads to missorting of MIG-14 to late endosomes and lysosomes (Yang *et al.*, 2008; Shi *et al.*, 2009; Harterink *et al.*, 2011). Loss of the retromer complex component SNX-1 disrupted the plasma membrane and Golgi localization of MIG-14::GFP and caused its accumulation on RAB-7–positive late endosomes and lysosomes (Supplemental Figure S3, A–C and F–H; Shi *et al.*, 2009). Like *ubc-13(tm3546)*, loss of *snx-1* did not affect MIG-14::GFP colocalization with RAB-10– or RME-8–positive endosomes (Supplemental Figure S3, D, E, I, and J; Shi *et al.*, 2009). We found that MIG-14::GFP appeared on the limiting membrane of RAB-7–positive late endosomes and lysosomes in *ubc-13(tm3546)*, but accumulated both in the RAB-7–labeled late endosomal/lysosomal lumen and on the limiting membrane in worms lacking retromer complex components SNX-1, VPS-29, VPS-26, or VPS-35 (Supplemental Figure S4). Moreover, MIG-14::GFP accumulation was significantly higher in *ubc-13;snx-1* and *ubc-13;vps-29(RNAi)* double mutants than in single mutants, indicating more severe defects in retrograde transport of MIG-14 (Figure 3, H–M). We observed both punctate and ring-like patterns of MIG-14::GFP in doubly defective *rab-10;snx-1(RNAi)* or *rab-10;vps26(RNAi)* worms, and the MIG-14 trafficking defects were additive in these animals (Supplemental Figure S3, K–Q). Altogether, these data further indicate that UBC-13 and the retromer complex promote retrograde transport of MIG-14 from endosomes to the Golgi, whereas RAB-10 acts through a distinct pathway to recycle MIG-14 from endosomes to plasma membranes. These results also suggest that MIG-14 missorted to late endosomes and lysosomes requires UBC-13 to reach the endosomal lumen.

Trafficking of retromer-dependent but not retromer-independent cargoes is impaired in *ubc-13(lf)* mutants

In addition to MIG-14, the glucose transporter GLUT-1 and the bone morphogenetic protein (BMP) type I receptor SMA-6 are also recycled in a retromer-dependent manner (Gleason *et al.*, 2014). Loss of the retromer complex component VPS-35 impaired recycling of GLUT-1 and SMA-6 to plasma membranes, leading to redistribution of the cargo to RAB-7–positive late endosomes and lysosomes (Figure 4, A–D, G–J, K–L″, N–O″, Q, and R; Gleason *et al.*, 2014). We found that loss of UBC-13 also affected trafficking of GLUT-1 and SMA-6, causing greatly reduced plasma membrane localization of GLUT-1 and significantly increased intracellular accumulation of both GLUT-1 and SMA-6 (Figure 4, E–J). In *ubc-13(tm3546)*, GLUT-1 and SMA-6 accumulated in the cytoplasm as tubules and ring-like structures that were labeled by RAB-7, suggesting that they are missorted to late endosomes and lysosomes like MIG-14 (Figure 4, M–M″, P–P″, Q, and R). By contrast, the pattern of hTfR, hTAC, and the BMP type II receptor DAF-4, which are recycled in a retromer-independent manner, was unaltered in *ubc-13(lf)* mutants (Supplemental Figure S5; Grant and Donaldson, 2009; Gleason *et al.*, 2014). These data indicate that UBC-13 is important for retrograde transport of retromer-dependent cargoes, but is dispensable for those that are recycled through retromer-independent pathways.

Loss of *ubc-13* disrupts the separation of recycling and degradation subdomains on endosomes

Ubc13 mediates K63-linked polyubiquitination, which is involved in a variety of processes including serving as a signal for sorting proteins into the MVE pathway (Lauwers *et al.*, 2010; Erpapazoglou *et al.*, 2014). The ESCRT machinery recognizes ubiquitinated cargoes and sorts them into ILVs of the endosome, leading to the formation of MVBs. We found that loss of *ubc-13* in both intestinal and hypodermal cells caused significantly enlarged vesicles labeled by HGRS-1, the ESCRT-0 subunit that binds PtdIns3P and ubiquitinated cargo on endosomes (Figure 5, A, B, and F, and Supplemental Figure S6, A–C). Similarly, RNAi inactivation of the ESCRT-I and -III components VPS-28 and VPS-20 led to enlargement of HGRS-1–positive vesicles (Supplemental Figure S6, D–F). Moreover, loss of UBC-13 or inactivation of HGRS-1 by RNAi led to significant enlargement of VPS-29–positive vesicles (Figure 5, C–E and G). Thus, ESCRT- and retromer-containing endosomes are affected in *ubc-13(lf)* mutants.

Retromer and ESCRT are thought to be present on the same endosome but are segregated into distinct microdomains (Raiborg *et al.*, 2002; Shi *et al.*, 2009). In *C. elegans* coelomocytes, SNX-1 and the DNAJ domain-containing protein RME-8 localize to distinct microdomains from HGRS-1 on endosomes and are required for maintaining the separation of the opposing functional subdomains, thus ensuring that recycling cargo is sorted away from the degradative pathway (Norris *et al.*, 2017). We found that HGRS-1 and SNX-1, which localized to distinct regions on a common endosome in wild-type coelomocytes, largely overlapped on abnormal endosomes in *ubc-13(tm3546)* mutants (Figure 5, K–L‴ and O). Similarly, in hypodermal cells, HGRS-1 and SNX-1 were separate in wild type but overlapped on enlarged endosomes in *ubc-13(tm3546)* (Figure 5, H–J). Moreover, the recycling cargo MIG-14 was enriched in endosomal regions distinct from HGRS-1 in wild-type coelomocytes, but overlapped with HGRS-1 on *ubc-13(tm3546)* endosomes (Figure 5, M–N‴ and P). These data collectively suggest that *ubc-13* function is important for the separation of the degradative and retrograde recycling subdomains on endosomes.

Subdomain separation and MIG-14 recycling defects are partially suppressed by expression of ubiquitin-tagged degradation-destined cargo in *ubc-13(lf)*

We have reported recently that UBC-13 acts with the U-box–containing E3 ligase CHN-1 to catalyze K63-linked ubiquitination on the class III PI3-kinase VPS-34, which is important for VPS-34 protein stability (Liu *et al.*, 2018). Loss of *ubc-13* or *chn-1* causes significantly reduced PtdIns3P on apoptotic cell–containing phagosomes, leading to defects in cell corpse degradation (Liu *et al.*, 2018). Unlike apoptotic cell–enclosing phagosomes, however, we found that PtdIns3P accumulation on endosomes was unaffected in *ubc-13(tm3546)* or *chn-1(by155)* worms (Supplemental Figure S6, G–I, K, L–N, and P). Moreover, loss of *chn-1*, which disrupts ubiquitin modification on VPS-34, did not affect MIG-14 trafficking. MIG-14::GFP was observed on basolateral membranes and appeared as small puncta in the cytoplasm of *chn-1(by155)* as in wild type (Supplemental Figure S7, A–D and G). In addition, HGRS-1 and SNX-1 localized

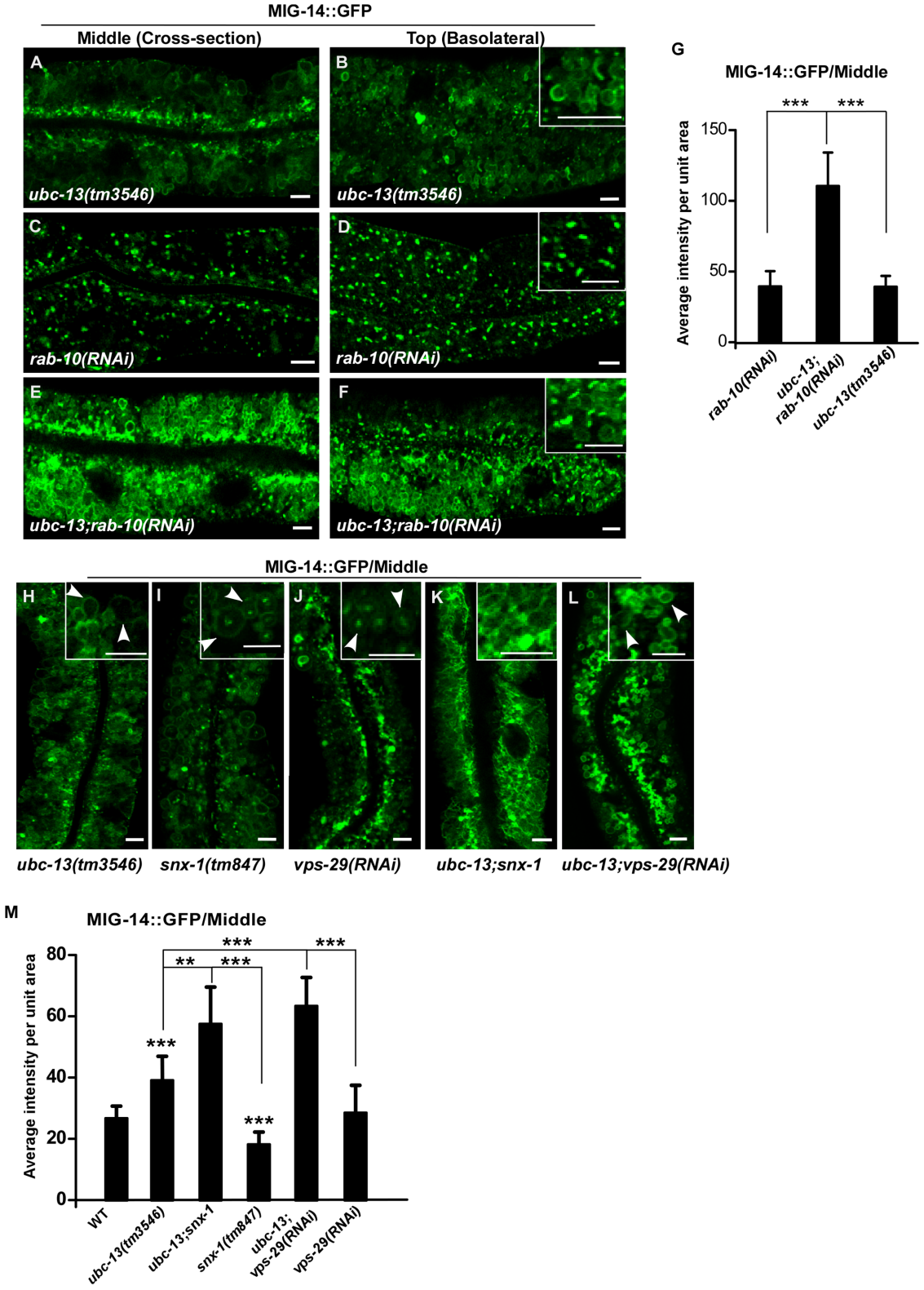

FIGURE 3: UBC-13 and RAB-10 act through distinct pathways to regulate MIG-14 trafficking. Confocal fluorescence images of the intestine at the middle (A, C, E, H–L) or the basolateral focal plane (B, D, F) in the indicated strains expressing MIG-14::GFP. MIG-14 accumulated as ring-like structures (arrowheads) in *ubc-13* and retromer complex mutants. Quantification of intracellular accumulation of MIG-14::GFP is shown in G and M. At least eight animals were quantified in each strain, and data are shown as mean ± SD. One-way ANOVA with Tukey's post hoc test was performed to compare data sets that are linked by lines. **, $P < 0.001$; ***, $P < 0.0001$. Scale bars: 5 μm.

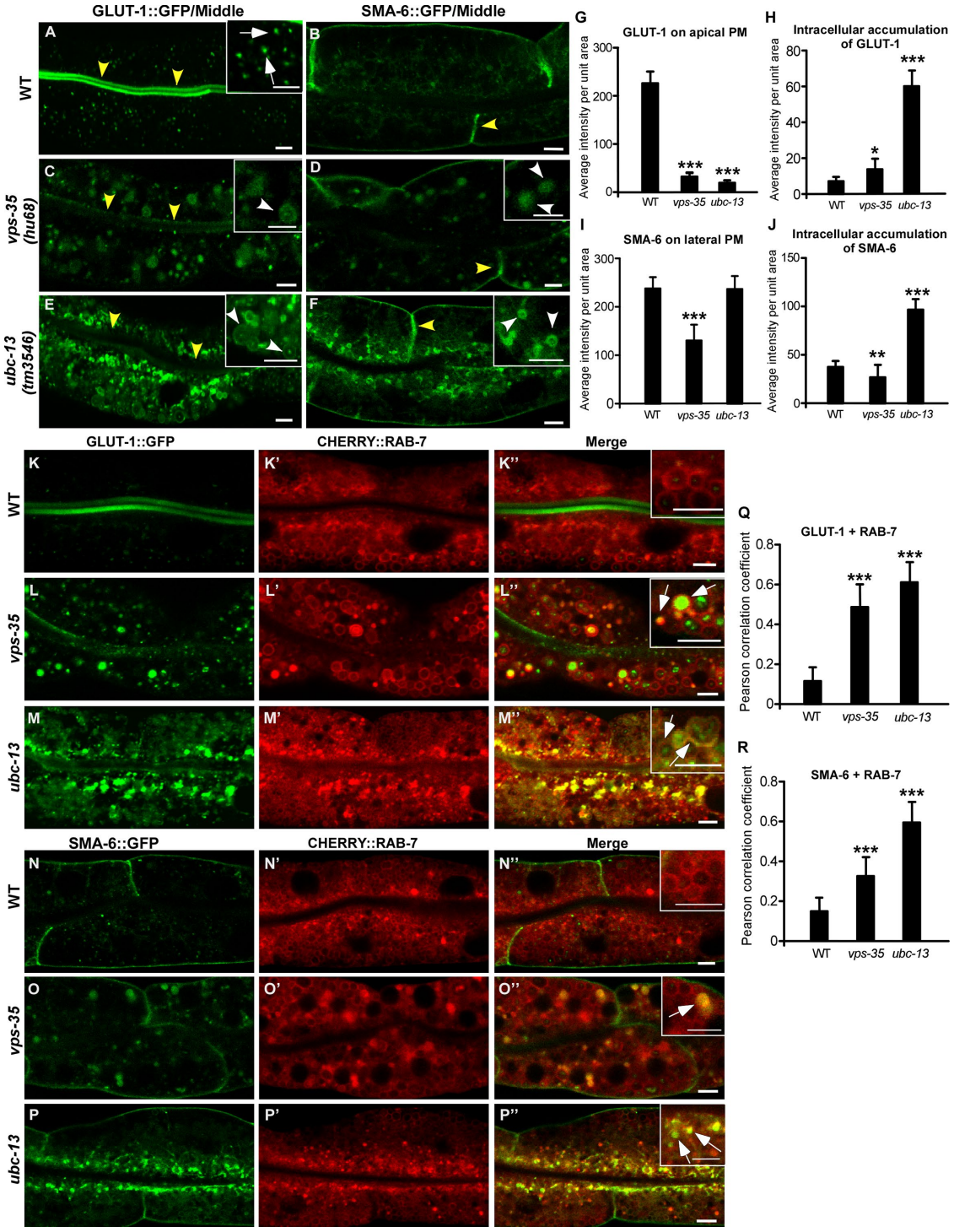

FIGURE 4: *ubc-13* affects recycling of the retromer-dependent cargoes GLUT-1 and SMA-6. (A–F) Confocal fluorescence images of the intestine in wild type (WT; A, B), *vps-35* (C, D), and *ubc-13* (E, F) expressing GLUT-1::GFP (A, C, E) or SMA-6::GFP (B, D, F). Yellow arrowheads indicate GFP labeling on apical or lateral membranes, white arrows designate GLUT-1::GFP puncta in the cytosol of wild-type worms, and white arrowheads indicate vesicular structures labeled by GLUT-1::GFP or SMA-6::GFP in the cytosol of *vps-35* and *ubc-13* mutants. (G–J) Quantification of the average fluorescence intensity of GLUT-1::GFP (G, H) and SMA-6::GFP (I, J) per unit area in different genetic backgrounds. (K–P″) Confocal fluorescence images of the intestine in wild-type (WT; K–K″, N–N″), *vps-35* (L–L″, O–O″), and *ubc-13* (M–M″, P–P″) animals coexpressing CHERRY::RAB-7 and GLUT-1::GFP (K–M″) or SMA-6::GFP (N–P″). Arrows indicate colocalization of GFP and CHERRY. (Q, R) Colocalization of CHERRY::RAB-7 and GLUT-1::GFP (Q) or SMA-6::GFP (R) was quantified in the indicated strains. In G–J and Q and R, at least eight animals were quantified in each strain, and data are shown as mean ± SD. One-way ANOVA with Tukey's post hoc test was performed to compare all the other data sets with wild type. *, $P < 0.05$; **, $P < 0.001$; ***, $P < 0.0001$. Scale bars: 5 μm.

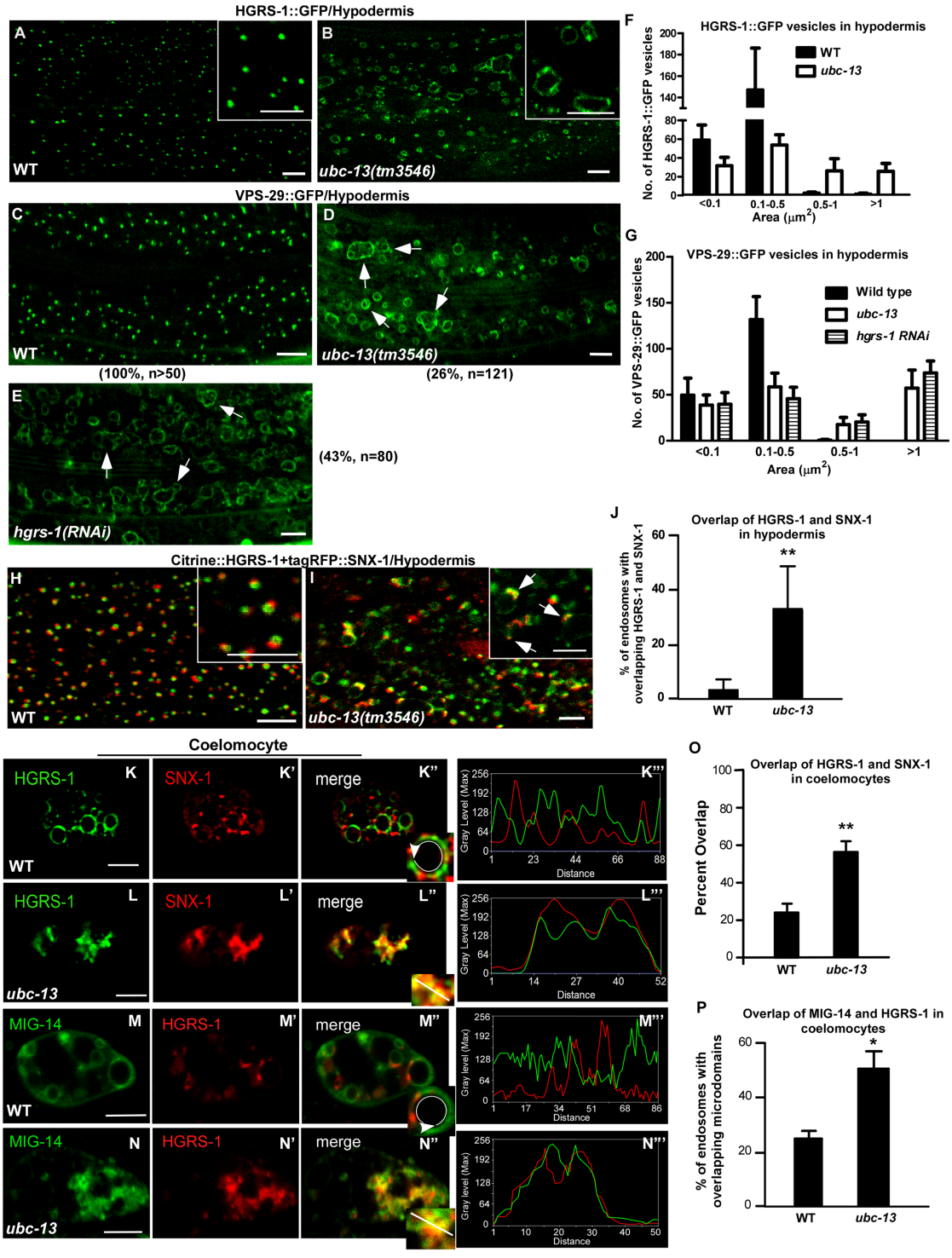

FIGURE 5: Loss of *ubc-13* affects separation of the SNX-1–retromer and the HGRS-1/ESCRT microdomains on endosomes. (A–E) Confocal fluorescence images of the hypodermis in wild type (WT; A, C), *ubc-13(tm3546)* (B, D), and *hgrs-1(RNAi)* (E) expressing HGRS-1::GFP (A, B) or VPS-29::GFP (C–E). Arrows indicate enlarged VPS-29::GFP-positive endosomes. The percentage of worms with the representative pattern is shown at the bottom (C, D) or side (E) of the image. (F, G) Size distribution of GFP-positive endosomes in the indicated strains. At least eight animals were quantified in each strain. (H–J) Confocal fluorescence images of the hypodermis in wild type (WT; H) and *ubc-13(tm3546)* (I) coexpressing Citrine::HGRS-1 and tagRFP::SNX-1. The overlap of HGRS-1 and SNX-1 on endosomes was quantified (J). (K–N″) Confocal fluorescence images of coelomocytes that coexpress Citrine::HGRS-1 and tagRFP::SNX-1 (K–L″) or MIG-14::GFP and HGRS-1::tagRFP (M–N″) in wild type and *ubc-13(tm3546)*. (K‴, L‴, M‴, N‴) The two-color line scan around the endosomal periphery is indicated by the white circles and lines in the insets of K″, L″, M″, and N″. Arrowheads indicate where the line scan starts and its direction. (O, P) Colocalization of HGRS-1 with SNX-1 (O) and MIG-14 with HGRS-1 (P) on endosomes was quantified. At least 10 animals were quantified in each strain. Significance was measured by Student's *t* test. *, $P < 0.05$; **, $P < 0.001$. Scale bars: 5 μm.

to distinct regions on endosomes in *chn-1(by155)*, indicating that microdomain separation is not affected (Supplemental Figure S7, H–O). These data suggest that disruption of VPS-34 ubiquitination does not affect PtdIns3P generation and subdomain separation on endosomes and has no effect on MIG-14 recycling.

We next examined endosomal PtdIns3P and MIG-14 recycling in *qx467* mutants, which carry a strong loss-of-function mutation in *vps-34* (Liu *et al.*, 2018). We found that PtdIns3P levels on endosomes were greatly reduced in *vps-34(qx467)*, and MIG-14 recycling was impaired (Supplemental Figure S6, J, K, O, and P, and Supplemental Figure S7, E–G). In addition, the number of HGRS-1– and SNX-1–positive puncta was greatly reduced in hypodermal cells, and SNX-1 appeared diffuse in the cytoplasm of *vps-34(qx467)* coelomocytes, consistent with the role of PtdIns3P in recruiting HGRS-1 and SNX-1 to endosomes (Supplemental Figure S7, J and N–N″). In the HGRS-1/SNX-1–positive puncta remaining in *vps-34(qx467)* hypodermis, the HGRS-1 and SNX-1 signals were separate, suggesting that subdomain separation is not disrupted (Supplemental Figure S7, J and K). Thus, while retrograde recycling and endosomal recruitment of sorting factors requires VPS-34, the regulation of VPS-34 by UBC-13 and CHN-1–mediated ubiquitination appears to have a dramatic effect on PtdIns3P generation on phagosomes but not endosomes. These results indicate that VPS-34 is not the UBC-13 substrate responsible for effects on retrograde recycling.

UBC-13 is also very important for K63-linked ubiquitination of cargoes destined for degradation in *C. elegans* embryos (Sato *et al.*, 2014). Consistent with this, we found that K63- but not K48-linked ubiquitin chains accumulated on endosomes in *hgrs-1(RNAi)* worms, and was abolished in *ubc-13;hgrs-1* double mutants (Supplemental Figure S8). We hypothesized that defective subdomain separation and retrograde recycling in *ubc-13(lf)* may be attributed to loss of cargo ubiquitination. To test this, we attempted to increase cargo ubiquitination in *ubc-13(lf)* by expressing a constitutively ubiquitinated cargo protein. CAV-1 is a worm homologue of caveolin that is modified with K63-linked ubiquitination by UBC-13 and delivered to lysosomes for degradation (Sato *et al.*, 2014). In *ubc-13(lf)* mutants, CAV-1 is not modified and is recycled to the cell surface instead of being targeted to the MVE pathway (Sato *et al.*, 2014). We found that expression of CAV-1::Ub, but not unubiquitinated CAV-1, in *ubc-13(tm3546)* mutants significantly reduced intracellular accumulation of MIG-14::GFP, especially accumulation of MIG-14–positive ring-like structures (Figure 6, A–H). Moreover, the abnormal overlap of HGRS-1 and SNX-1 on endosomes of *ubc-13(tm3546)* mutants was suppressed in animals expressing CAV-1::Ub, but not the unubiquitinated CAV-1 control protein, suggesting that separation of degradative and recycling subdomains on endosomes requires the presence of ubiquitinated transmembrane cargo (Figure 6, I–L). Importantly, expression of CAV-1::Ub led to a reappearance of MIG-14::GFP on MANS-positive puncta (Figure 6, M–O), which indicates restoration of MIG-14 recycling from endosomes to the Golgi apparatus, consistent with the idea that subdomain separation is important for recycling function.

UBC-13 acts in EGL-20/Wnt–producing cells to regulate MIG-14 trafficking and Wnt-dependent processes

UBC-13 is widely expressed in multiple cell types including cells that produce EGL-20/Wnt (Supplemental Figure S1, K and K′). Indeed, we observed expression of GFP controlled by the *ubc-13* promoter in cells expressing $P_{egl\text{-}20}$CHERRY, indicating that *ubc-13* is expressed in EGL-20/Wnt–producing cells (Figure 7, A–A″). In wild type, the majority of MIG-14::GFP localized to the plasma membranes in EGL-20/Wnt–producing cells, and a small proportion of the GFP signal was observed in intracellular membranes (Figure 7, B, F, and G). In *ubc-13(tm3546)*, however, there was a significant reduction in the level of MIG-14::GFP on plasma membranes and a concomitant increase in intracellular MIG-14 accumulation (Figure 7, C, F, and G). A similar effect was observed in mutants with loss of the retromer complex component VPS-29 (Figure 7, D, F, and G). The reduction in the level of MIG-14 on the plasma membrane was significantly more severe in *vps-29;ubc-13* double mutants (Figure 7, D–G). In *vps-29;ubc-13*, MIG-14::GFP was absent from plasma membranes but accumulated as small puncta in intracellular membranes (Figure 7, E and F). Thus, as in the intestine, loss of both UBC-13 and the retromer complex component causes more severe defects in MIG-14 recycling in EGL-20/Wnt–producing cells that require MIG-14 for EGL-20/Wnt secretion.

We next examined whether Wnt signaling is affected in *ubc-13(lf)* mutants that are defective in MIG-14/Wntless trafficking. In the first stage of larval development, the left Q neuroblast (QL) and its descendants (QL.ds) migrate from the midbody to well-defined positions in the posterior (Sulston and Horvitz, 1977). Loss of EGL-20/Wnt leads to abnormal migration of QL.ds toward the anterior region (Figure 7H; Harris *et al.*, 1996). We found that migration of PVM, one of the QL cell descendants labeled by $P_{mec\text{-}4}$GFP, was not affected in *ubc-13* or *vps-29* single mutants, whereas 98% of *vps-29;ubc-13* double mutants contained mismigrated PVM (Figure 7I). In *vps-29;ubc-13*, PVM adopted an anterior position instead of migrating to the posterior region, a phenotype similar to *egl-20(n585)* (Figure 7H; Harris *et al.*, 1996; Pan *et al.*, 2008). Moreover, anterior migration of HSN neurons, which is defective in Wnt mutants, was also affected in *vps-29;ubc-13* worms (Supplemental Figure S9, A and B; Pan *et al.*, 2006). The PVM migration defect in *vps-29;ubc-13* was rescued by expressing *ubc-13* or *vps-29* driven by endogenous promoters or the *egl-20* promoter, suggesting that UBC-13 and retromer act cell-autonomously to regulate Wnt signaling (Figure 7I). The additive Wnt phenotypes are consistent with enhanced defects in MIG-14 trafficking in *vps-29;ubc-13*, which suggests that UBC-13 and retromer complex act coordinately to mediate Wnt signaling by regulating retrograde transport of MIG-14/Wntless.

DISCUSSION

UBC-13 function is required for retrograde transport of retromer-dependent cargoes

K63-linked polyubiquitination catalyzed by the E2 ubiquitin-conjugating enzyme Ubc13 is important for endocytosis and for sorting of cargoes into the degradative multivesicular endosome pathway (Tanno and Komada, 2013; Erpapazoglou *et al.*, 2014). Loss of UBC-13–dependent K63-linked ubiquitination in *C. elegans* disrupts lysosomal clearance of maternal membrane proteins, causing recycling of the degradative cargo to the cell surface (Sato *et al.*, 2014). Unexpectedly, we found here that UBC-13 is also required for retromer-dependent recycling, thus placing UBC-13 at the center of the endosomal sorting process. Our data indicate that UBC-13 is essential for retrograde transport of retromer-dependent cargoes, including the Wnt transporter MIG-14/Wntless, the glucose receptor GLUT-1, and the BMP receptor SMA-6. In this process, UBC-13 acts in a cell-autonomous manner and its function requires E2 ubiquitin-conjugating activity, implicating the K63 ubiquitination activity of UBC-13 in the retrograde transport process. Loss of *ubc-13* did not affect uptake of MIG-14 from the plasma membrane, but clearly disrupted its transport from endosomes to the Golgi, causing missorting of MIG-14 to late endosomes and lysosomes. This phenotype closely resembled, and was enhanced by retromer complex mutations, suggesting that UBC-13 and retromer complex work together in this

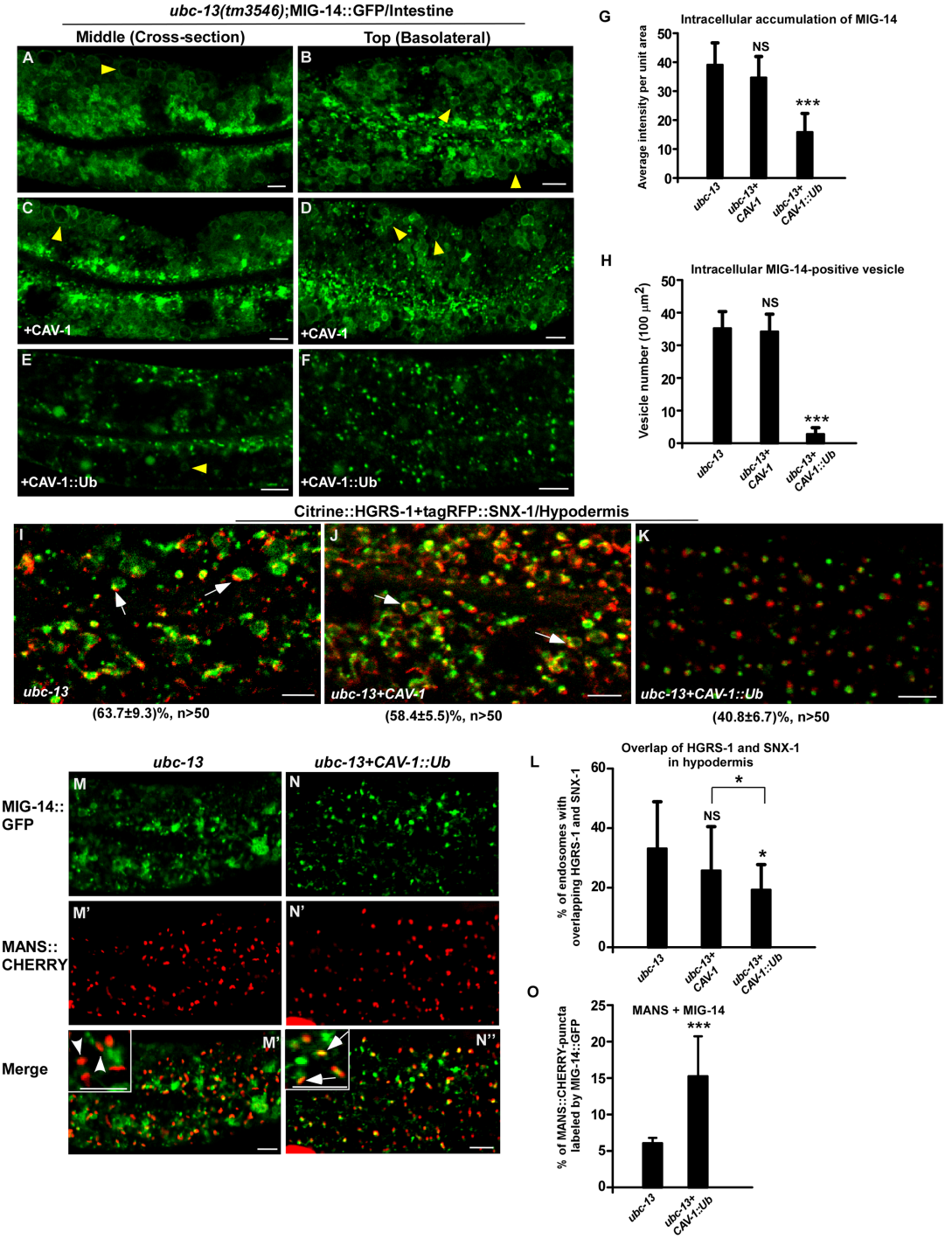

FIGURE 6: Expression of CAV-1::Ub partially restores microdomain separation and MIG-14 recycling in *ubc-13(lf)*. (A–F) Confocal fluorescence images of the intestine at the middle or the basolateral focal plane in *ubc-13(tm3546)* expressing MIG-14::GFP without (A, B) or with expression of CAV-1 (C, D) or CAV-1::Ub (E, F) in the intestine. Intracellular accumulation of MIG-14::GFP and average number of MIG-14–positive vesicles (arrowheads) in a 100-μm^2 region were quantified (G, H). At least eight animals were quantified in each strain. (I–K) Confocal fluorescence images of the hypodermis in *ubc-13(tm3546)* coexpressing Citrine::HGRS-1 and tagRFP::SNX-1 without (I) or with (J) expression of CAV-1 or CAV-1::Ub (K) in the hypodermis. The percentage of worms with the representative pattern is shown at the bottom of the image. Arrows indicate overlap of HGRS-1 and SNX-1 on endosomes that was quantified in L. At least eight animals were scored in each strain, and data are shown as mean ± SD. (M–N″) Confocal fluorescence images of the intestine in *ubc-13(tm3546)* animals coexpressing MIG-14::GFP and MANS::CHERRY without (M–M″) or with (N–N″) expression of CAV-1::Ub in the intestine. Arrows indicate colocalization of GFP and CHERRY. Arrowheads indicate puncta that are labeled by MANS::CHERRY but not MIG-14::GFP. Colocalization of MIG-14::GFP with MANS::CHERRY was quantified in O. At least five animals were scored in each strain, and data are shown as mean ± SD. One-way ANOVA with Tukey's post hoc (G, H, L) and Student's *t* test (O) were performed to compare all the other data sets with *ubc-13* or data sets that are linked by lines. *, $P < 0.05$; ***, $P < 0.0001$. N.S.: no significance. Scale bars: 5 μm.

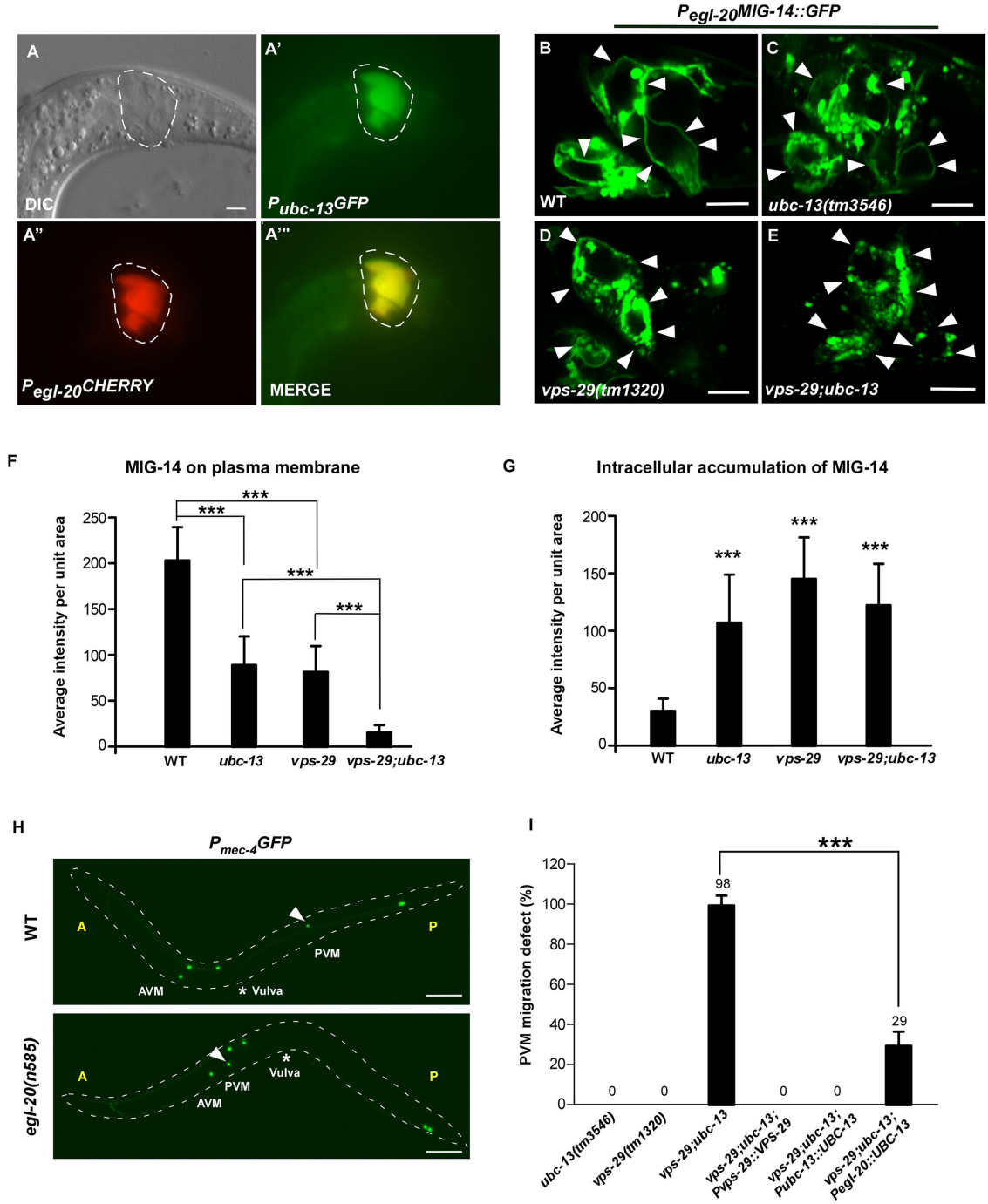

FIGURE 7: UBC-13 functions in EGL-20/Wnt–producing cells to regulate MIG-14 trafficking and Wnt signaling. (A–A‴) DIC and fluorescence images of EGL-20–producing cells (dashed circles) coexpressing GFP and CHERRY driven by *ubc-13* and *egl-20* promoters, respectively. (B–E) Confocal fluorescence images of MIG-14::GFP driven by the *egl-20* promoter in wild type (WT; B), *ubc-13(tm3546)* (C), *vps-29(tm1320)* (D), and *vps-29;ubc-13* (E). Arrowheads indicate the plasma membrane labeled by MIG-14::GFP. (F, G) Quantification of MIG-14::GFP on plasma membranes (F) and in the cytosol (G) of EGL-20–producing cells in the indicated strains. At least eight animals were quantified. (H) Fluorescence images of GFP controlled by the *mec-4* promotor in wild type and *egl-20(n585)*. The two Q neuroblast descendants AVM and PVM are labeled by GFP. Arrowheads point to PVM cells, and asterisks indicate the vulva region. (I) The migration of QL.ds was quantified in the indicated strains. At least 100 worms were quantified. In F, G, and I, data are shown as mean ± SD. One-way ANOVA with Tukey's post hoc test was performed to compare data sets that are linked by lines. ***, $P < 0.0001$. Scale bars indicate 5 μm in A–E and 50 μm in H.

process. These effects were specific because loss of UBC-13 disrupts trafficking of retromer-dependent cargoes but is dispensable for trafficking of cargoes that are recycled through retromer-independent pathways. We found that RAB-10, a key regulator of the basolateral recycling pathway, also participates in MIG-14 trafficking in the intestine, but it acts through a distinct pathway from UBC-13 and retromer to recycle MIG-14 from endosomes to the plasma membrane.

Cargo ubiquitination by UBC-13 is important for maintaining functionally distinct microdomains on endosomes

The retromer complex directs cargo from endosomes to the Golgi for recycling and the ESCRT machinery sorts ubiquitinated cargo into the MVE pathway for lysosomal degradation. These two distinct activities, however, are thought to occur on the same endosome but are separated into different microdomains. Hrs, an ESCRT-0 component, has been reported to bind endosomal clathrin, and to be organized into a microdomain by endosomal clathrin (Raiborg *et al*., 2001b, 2006). The Hrs- and clathrin-microdomain organizes degradation of transmembrane cargoes, and is distinct from microdomains containing retromer-associated components such as VPS-35, SNX-1, or RME-8 (Raiborg *et al*., 2001a, 2002, 2006; Sachse *et al*., 2002; Norris *et al*., 2017). Retromer-associated SNX-1 and its interacting protein RME-8 are required to maintain separation of retromer and HGRS-1/Hrs subdomains. Current models posit that SNX-1 and RME-8 regulate clathrin disassembly on endosomes to restrict the HGRS-1/Hrs degradative microdomains, preventing their encroachment on recycling microdomains. This promotes proper sorting of recycling cargoes and helps to prevent their inappropriate degradation (Shi *et al*., 2009; Norris *et al*., 2017). Here we found that loss of *ubc-13*, the E2 ubiquitin-conjugating enzyme responsible for generating K63-linked ubiquitin chains, also disrupted microdomain separation, leading to mixing of HGRS-1/Hrs– and SNX-1–positive domains on endosomes. This indicates that K63-linked polyubiquitination, which serves as a sorting tag for cargo entry into the degradative pathway, is important for maintaining the functionally distinct microdomains on endosomes.

Our data suggest that VPS-34, the class III PI3-kinase modified by UBC-13 (E2) and CHN-1 (E3), is not the key substrate of UBC-13 in retrograde recycling. On the other hand, loss of *ubc-13* disrupts accumulation of K63-linked ubiquitin chains on endosomes in *hgrs-1(RNAi)* worms, and expression of ubiquitin-tagged degradation-destined cargo partially suppresses microdomain separation defects and MIG-14 recycling defects in *ubc-13(lf)* mutants. These data suggest that cargo ubiquitination mediated by UBC-13 is important for subdomain separation.

Hrs binds directly to both ubiquitin and clathrin to sort ubiquitinated membrane proteins into clathrin-coated degradative microdomains (Raiborg *et al*., 2002). Hrs contains a double-sided ubiquitin-interacting motif that is capable of binding two ubiquitin molecules (Hirano *et al*., 2006). Hrs associates with STAM (signal transducing adaptor molecule) to form a heterotetrameric ESCRT-0 complex that contains eight ubiquitin-binding sites and exhibits stronger affinity for polyubiquitin chains than for monoubiquitin (Ren and Hurley, 2010; Mayers *et al*., 2011). Thus, clustering of K63-linked ubiquitinated cargoes with HGRS-1/Hrs may promote formation and/or maintenance of the degradative microdomain, which ensures efficient segregation of degradative cargoes from the recycling cargo. Consistent with this model, we found that loss of *ubc-13* disrupts microdomain separation, causing missorting of the recycling cargoes into the degradative pathway, and these phenotypes are partially suppressed by expression of a ubiquitin-tagged degradation-destined cargo. The MIG-14 recycling phenotype caused by *ubc-13(lf)* resembles and is enhanced by SNX-1–retromer complex mutations. Thus, the retrograde transport pathway and the degradative pathway, which are spatially separated into distinct subdomains on endosomes, coordinate to direct cargo sorting to different destinations. In line with this, both clathrin and Hrs have been implicated in retrograde sorting on endosomes, although their precise roles remain to be elucidated (Lauvrak *et al*., 2004; Saint-Pol *et al*., 2004; Popoff *et al*., 2007, 2009). Our results suggest that intermixing of ESCRT complexes with retromer may be the root cause of recycling defects in *ubc-13* mutants, and that retromer function may require separation from ESCRT.

We found that HGRS-1– and VPS-29–positive vesicles were significantly enlarged in *ubc-13(lf)* mutants, and MIG-14::GFP, which is missorted to the degradative pathway, stayed on the limiting membrane of RAB-7–positive vesicles instead of being present in the lumen, leading to persistence but not degradation of MIG-14. This suggests that ILV formation may be impaired in *ubc-13(lf)*, which is consistent with the essential role of cargo ubiquitination in ILV formation in yeast (MacDonald *et al*., 2012). Thus, K63-linked ubiquitination is important for cargo selection in both degradative and retrograde transport pathways.

Requirement for the E2 ubiquitin-conjugating enzyme UBC-13 in Wnt signaling

Our data indicate that UBC-13 is important for MIG-14/Wntless trafficking not only in polarized intestinal cells but also in EGL-20/Wnt–producing cells. Consistent with this, loss of both UBC-13 and retromer components disrupted EGL-20/Wnt–dependent processes in a cell-autonomous manner. Our finding reveals a novel requirement for the E2 ubiquitin-conjugating enzyme UBC-13/Ubc13 in Wnt signaling and suggests that Ubc13 may be widely involved in signaling processes by regulating both retrograde recycling and degradation of membrane proteins.

MATERIALS AND METHODS

C. elegans strains

Strains of *C. elegans* were cultured and maintained using standard protocols (Brenner, 1974). The N2 Bristol strain was used as the wild-type strain. Standard microinjection methods were used to generate transgenic animals carrying extrachromosomal arrays (*qxEx*), and genome-integrated arrays (*qxIs*) were acquired by γ-irradiation to achieve stable expression from arrays with low copy numbers. Strains that were used in this work are summarized in Supplemental Table S1.

RNAi

RNAi was performed by using the standard feeding method. For most experiments, 5–10 L4 larvae (P0) were cultured on the RNAi plate and F1 progeny at the L4 stage were examined. For *hgrs-1*, *vps-20*, *and vps-28 RNAi*, 30 L1 larvae were cultured on RNAi plates and the phenotype was checked 48 h after L4 at the same generation because most F1 progeny die before reaching the adult stage as a result of inactivation of *hgrs-1*, *vps-20*, and *vps-28*.

Microscopy and image analysis

Worms were mounted on 4% agarose pads with 10 mM levamisole for imaging. Differential interference contrast (DIC) and fluorescence images were captured with an Axioimager A1 microscope (Carl Zeiss) equipped with epifluorescence (Filter Set 13 for GFP [excitation BP 470/20, beam splitter FT 495, emission BP 503–530] and Filter Set 20 for Cherry [excitation BP 546/12, beam splitter FT 560, emission BP 575–640]) and an AxioCam monochrome digital camera (Carl Zeiss). Confocal microscopy images were taken by an inverted confocal microscope (LSM 5 Pascal, LSM 880; Carl Zeiss) with 488 (emission filter BP 503–530) and 543 (emission filter BP 560–615) lasers used. Images were processed and viewed using LSM Image Browser software (Carl Zeiss). All images were taken at 20°C.

Quantification of cargo accumulation and colocalization analyses

Fluorescence intensity was measured by ImageJ 1.42q (National Institutes of Health). To quantify accumulation of MIG-14, GLUT-1,

SMA-6, DAF-4, hTAC, and hTfR in the intracellular membranes of intestinal cells, the average fluorescence intensity per unit area of three regions (50 μm^2 each using the "Rectangular selections" tool) was measured in each L4 larva and eight animals were scored in each strain. The regions for measurement were selected without regard to the density of labeled objects. To quantify cargo accumulation on the plasma membrane in intestinal cells, the average fluorescence intensity of 10 points (using the "Point selections" tool) on the plasma membrane was measured in each L4 larva and eight animals were scored in each strain. To quantify the number of MIG-14–positive vesicles in the intestine, three regions were selected (100 μm^2 each using the "Rectangular selections" tool) and the average number was quantified in each L4 larva and at least eight animals were scored in each strain.

MIG-14 accumulation in EGL-20–producing cells was quantified in L4 larvae. The intracellular accumulation was quantified by first selecting the total cytosolic region inside the plasma membranes using the "Freehand line selections" tool followed by measurement of the average intensity per unit area. To determine MIG-14 accumulation on plasma membranes, the "Point selections" tool was used to select 10 points on the plasma membrane in each cell. All EGL-20–producing cells were quantified in each animal and at least eight animals were scored in each strain.

The colocalization of MIG-14::GFP with CHERRY::RME-8, MANS::CHERRY, or CHERRY::RAB-7 was quantified in L4 larvae. A 250 μm^2 area was selected and the percentage of CHERRY-positive structures that were labeled by MIG-14::GFP was determined. Three areas were selected without regard to the density of labeled objects in each animal and at least five animals were quantified in each strain. To quantify colocalization of CHERRY::RAB-7 and GLUT-1::GFP or SMA-6::GFP, images were analyzed by Velocity software and the Pearson correlation coefficient was determined. At least eight animals were quantified in each strain.

To measure the area of HGRS-1::GFP– and VPS-29::GFP–positive vesicles, images were captured in worms 48 h post L4 with an equal exposure time. The images were analyzed by Velocity software and quantified using the "Find Object" function under equal threshold. At least eight animals were quantified in each strain. The area of VPS-29::GFP–positive structures was quantified in *ubc-13(tm3546)* and *hgrs-1(RNAi)* worms containing enlarged GFP-positive vesicles.

Examination of microdomain separation on endosomes

Colocalization of Citrine::HGRS-1 and tagRFP::SNX-1 in the hypodermis was quantified in L4 larvae. Images were captured with an equal exposure time and intensities in each channel were thresholded equally. A 250-μm^2 area was selected and the percentage of endosomes with overlapping HGRS-1 and SNX-1 was determined manually. Three areas were selected without regard to the density of labeled objects in each animal and at least eight animals were quantified in each strain. Colocalization of Citrine::HGRS-1 and tagRFP::SNX-1 on endosomes in coelomocytes was determined as previously described (Norris *et al.*, 2017). To quantify the overlap of MIG-14::GFP and HGRS-1::tagRFP in coelomocytes, images were analyzed by Velocity software and intensities in each channel were thresholded. Endosomes that were labeled by both MIG-14::GFP and HGRS-1::RFP were scored. Endosomes with overlapping intensity peaks of MIG-14::GFP and HGRS-1::RFP were scored as positive for overlapping microdomains. At least 10 animals were scored, and an average of three independent experiments is shown in Figure 5P. Endosomes in *ubc-13* coelomocytes usually collapsed together and one cluster was scored as one endosome. Thus, the percentage of endosomes with overlapping microdomains in *ubc-13* was likely underestimated.

Examination of Q cell and HSN neuron migration

The Q descendant AVM and PVM neurons were labeled by P_{mec-4}-GFP and migration of Q cells was analyzed at the L4 stage. Animals in which PVM was located anterior of the vulva were scored as defective in Q cell migration. More than 100 animals were quantified in each strain, and an average of three independent experiments is shown in Figure 6I. The HSN neurons were labeled by P_{tph-1}GFP and their migration was examined in L4 larvae. Animals in which HSN neurons were located in a position where the vertical distance to the vulva was longer than the diameters of 10 HSN cell bodies were scored as defective in HSN migration. More than 50 animals were quantified in each strain, and an average of three independent experiments is shown in Supplemental Figure S4H.

Immunostaining

Dissected intestines were fixed sequentially in 4% paraformaldehyde for 10 min and in methanol at –20°C for 5 min. Fixed intestines were then blocked with PTBS (phosphate-buffered saline [PBS] containing 0.1% Tween 20, 2% bovine serum albumin [BSA], 10% serum) and incubated with anti-polyubiquitin antibodies specific for K48 and K63 linkages (Apu2, Apu3; Millipore), respectively, in blocking solution at 4°C overnight. Samples were washed three times in PTB (PBS containing 0.1% Tween 20, 2% BSA) and stained with the secondary antibody at room temperature before examination.

Statistical analysis

The SD was used as *y*-axis error bars for bar charts plotted from the mean value of the data. Data derived from different genetic backgrounds were compared by Student's two-tailed unpaired *t* test, one-way analysis of variance (ANOVA), followed by Tukey's post hoc test or two-way ANOVA followed by Bonferroni *post* hoc test as indicated in the figure legends. Data were considered statistically different at $P < 0.05$. $P < 0.05$ is indicated with single asterisks, $P < 0.001$ with double asterisks, and $P < 0.0001$ with triple asterisks.

Plasmid construction

To construct P_{ubc-13}GFP, 2.7 kb genomic sequence upstream of the *ubc-13* start codon ATG was amplified using primers PJCL290/PJCL291 and cloned into pPD49.26-GFP1 through the *Sph*I and *Xma*I sites. To generate P_{egl-20}CHERRY, 1.9 kb genomic sequence upstream of the start codon of *egl-20* was amplified using primers PJHY119/PJHY120 and inserted into pPD49.26-CHERRY1 through the *Bam*HI site. To construct P_{ubc-13}UBC-13, UBC-13 genomic sequence was amplified using primers PJCL287/PJCL288 and cloned into P_{ubc-13}GFP1 through the *Xma*I and *Nhe*I sites. To generate P_{vha-6}UBC-13 and P_{egl-20}UBC-13, the promoter region of *vha-6* and *egl-20* was cloned into P_{ubc-13}UBC-13 through the *Xma*I and *Nhe*I sites to replace the *ubc-13* promoter. To generate P_{ubc-13}UBC-13(C88G), the C to G mutation was introduced into UBC-13 by site-directed mutagenesis using primers PJCL413 and PJCL414. To construct P_{egl-20}MIG-14::GFP, the *egl-20* promoter was cloned into pPD49.26-GFP3 through the *Bam*HI site, then the genomic sequence of MIG-14, amplified by primers PJHY121/PJHY122, was inserted through the *Xma*I and *Kpn*I sites. To construct P_{vha-6}CAV-1::Ub and P_{hyp-7}CAV-1::Ub, the genomic sequence of CAV-1 and UBQ-2 was amplified using primers PJBZ541/PJBZ542 and PJBZ543/P JBZ544, respectively, and cloned into pPD49.26-P_{vha-6} or pPD49.26-P_{hyp-7} using the "seamless cloning" method. See Table 1 for the primers used.

Primer	Sequences (5′ to 3′)
PJBZ157	TTACCGCAGGATCCTATTGTGA
PJBZ158	CCAGATTTTTGACGGAACTACG
PJBZ159	AAATGAAGGGGTTGTTGG
PJBZ174	GGAATTCCATATGGCGGGCGGAGCCGTCAT
PJBZ175	CGCCCCGGGTCAATCGGTGCTCGGCTTC
PJBZ184	AATTTCTTCGTAATTTCTTTCTGT
PJBZ233	CGCCCCGGGATGGTAATAAATCAAATTAT
PJBZ234	CTAGCTAGC TTATGTGGTCTTCGATTTC
PJBZ235	CTAGCTAGC TGTGGTCTTCGATTTCTTG
PJBZ236	AACTGCAGAAGTTTCCCTTTTATTTTTGAAGTCATCC
PJBZ237	CGCCCCGGGTATTTCTGAAATTGAGATGTTTTAGAATTTC
PJBZ541	AGGAGGACCCTTGGCTAGCGTCGACATGTCCACCGAGCAAGATATCAAGA
PJBZ542	TGATCCTCCACCTCCTGATCCTCCACCTCCGACGCATGGAGCAGTAGTTTCTTGA
PJBZ543	GGAGGTGGAGGATCAGGAGGTGGAGGATCAATGCAAATCTTCGTCAAGACTCTGA
PJBZ544	TGCGGAGCTCAGATATCAATACCATTTATCCTCCACGAAGACGGAGCACC
PJCL287	CGCCCCGGGATGGCCGGGCAACTTCCGCGTCG
PJCL288	CGCGCTAGCTCAGGCTTCTGAAAAAAAATTATT
PJCL290	CGCACTAGTAGGTTCTGGACGATGTGATGGC
PJCL324	CCATTTGCTGGTGGTGTCTTC
PJCL325	TACATTTTCGCAGTTTCTTTG
PJCL414	CCTTGAGAATATCGAGACCAATTCTGCCGAGTTTATCAATATTCGGATG
PJCL470	TACTCTGCTGTACTGTCCGCTTC
PJCL471	CCATTGCTCTGATTGACTCCC
PJCL472	ATCCGAATCAAACCGTGTACC
PJCL473	GTCATATCGCTGTCATCCTCC
PJHY119	CGCGGATCCGTTTCCCTTTTATTTTTGAA
PJHY120	CGCGGATCCTATTTCTGAAATTGAGATGT
PJHY121	TCCCCCCGGGATGGCGGGCGGAGCCGTCAT
PJHY122	CGGGGTACCATCGGTGCTCGGCTTCAGGA
PWX8	GGAAATGTTGTCGGAAGAGGA
PWX9	GAAAAAGGGATAAGCGTCAGG
PWZ13	CACTAGCATATGTCGGGAACCAGAAAGAAGGCGC
PWZ14	GCGGATCCTTAACAATTGCATCCCGAATTCTG
PWZ23	CACTAGCATATGACGGCTGCTCCTTACAATTATTC
PWZ24	GCGGATCCCTAGCAGTTGCAGTCCTTCTTCCCAT

TABLE 1: Primers used for plasmid construction.

ACKNOWLEDGMENTS

We thank R. Legouis (Institute for Integrative Biology of the Cell), Ji Ying Sze (Albert Einstein College of Medicine), C. Yang (Yunnan University), G. Ou (Tsing University), and S. Mitani (Tokyo Women's Medical University) for strains and Isabel Hanson for editing services. Some strains were provided by the Caenorhabditis Genetics Center (CGC), which is funded by the National Institutes of Health (NIH) Office of Research Infrastructure Programs (P40OD010440). This work was supported by NIH Grants no. GM-067237 and GM-103995 to B.D.G. and the Ministry of Science and Technology (2016YFA0500203), the National Science Foundation of China (31325015, 3163001), the Strategic Priority Research Program of the Chinese Academy of Sciences (XDB19000000), and an International Early Career Scientist grant from the Howard Hughes Institute to X.W.

REFERENCES

Babbey CM, Ahktar N, Wang E, Chen CC, Grant BD, Dunn KW (2006). Rab10 regulates membrane transport through early endosomes of polarized Madin-Darby canine kidney cells. Mol Biol Cell 17, 3156–3175.

Banziger C, Soldini D, Schutt C, Zipperlen P, Hausmann G, Basler K (2006). Wntless, a conserved membrane protein dedicated to the secretion of Wnt proteins from signaling cells. Cell 125, 509–522.

Bartscherer K, Pelte N, Ingelfinger D, Boutros M (2006). Secretion of Wnt ligands requires Evi, a conserved transmembrane protein. Cell 125, 523–533.

Belenkaya TY, Wu Y, Tang X, Zhou B, Cheng L, Sharma YV, Yan D, Selva EM, Lin X (2008). The retromer complex influences Wnt secretion by recycling wntless from endosomes to the trans-Golgi network. Dev Cell 14, 120–131.

Belgareh-Touze N, Leon S, Erpapazoglou Z, Stawiecka-Mirota M, Urban-Grimal D, Haguenauer-Tsapis R (2008). Versatile role of the yeast ubiquitin ligase Rsp5p in intracellular trafficking. Biochem Soc Trans 36, 791–796.

Bonifacino JS, Hurley JH (2008). Retromer. Curr Opin Cell Biol 20, 427–436.

Brenner S (1974). The genetics of *Caenorhabditis elegans*. Genetics 77, 71–94.

Burd C, Cullen PJ (2014). Retromer: a master conductor of endosome sorting. Cold Spring Harb Perspect Biol 6, a016774.

Carlton J, Bujny M, Peter BJ, Oorschot VM, Rutherford A, Mellor H, Klumperman J, McMahon HT, Cullen PJ (2004). Sorting nexin-1 mediates tubular endosome-to-TGN transport through coincidence sensing of high-curvature membranes and 3-phosphoinositides. Curr Biol 14, 1791–1800.

Chen CC, Schweinsberg PJ, Vashist S, Mareiniss DP, Lambie EJ, Grant BD (2006). RAB-10 is required for endocytic recycling in the *Caenorhabditis elegans* intestine. Mol Biol Cell 17, 1286–1297.

Duncan LM, Piper S, Dodd RB, Saville MK, Sanderson CM, Luzio JP, Lehner PJ (2006). Lysine-63-linked ubiquitination is required for endolysosomal degradation of class I molecules. EMBO J 25, 1635–1645.

Erpapazoglou Z, Dhaoui M, Pantazopoulou M, Giordano F, Mari M, Leon S, Raposo G, Reggiori F, Haguenauer-Tsapis R (2012). A dual role for K63-linked ubiquitin chains in multivesicular body biogenesis and cargo sorting. Mol Biol Cell 23, 2170–2183.

Erpapazoglou Z, Walker O, Haguenauer-Tsapis R (2014). Versatile roles of k63-linked ubiquitin chains in trafficking. Cells 3, 1027–1088.

Franch-Marro X, Wendler F, Guidato S, Griffith J, Baena-Lopez A, Itasaki N, Maurice MM, Vincent JP (2008). Wingless secretion requires endosome-to-Golgi retrieval of Wntless/Evi/Sprinter by the retromer complex. Nat Cell Biol 10, 170–177.

Gleason RJ, Akintobi AM, Grant BD, Padgett RW (2014). BMP signaling requires retromer-dependent recycling of the type I receptor. Proc Natl Acad Sci USA 111, 2578–2583.

Goodman RM, Thombre S, Firtina Z, Gray D, Betts D, Roebuck J, Spana EP, Selva EM (2006). Sprinter: a novel transmembrane protein required for Wg secretion and signaling. Development 133, 4901–4911.

Grant BD, Donaldson JG (2009). Pathways and mechanisms of endocytic recycling. Nat Rev Mol Cell Biol 10, 597–608.

Gu M, Liu Q, Watanabe S, Sun L, Hollopeter G, Grant BD, Jorgensen EM (2013). AP2 hemicomplexes contribute independently to synaptic vesicle endocytosis. Elife 2, e00190.

Haglund K, Dikic I (2012). The role of ubiquitylation in receptor endocytosis and endosomal sorting. J Cell Sci 125, 265–275.

Harris J, Honigberg L, Robinson N, Kenyon C (1996). Neuronal cell migration in *C. elegans*: regulation of Hox gene expression and cell position. Development 122, 3117–3131.

Harterink M, Port F, Lorenowicz MJ, McGough IJ, Silhankova M, Betist MC, van Weering JRT, van Heesbeen R, Middelkoop TC, Basler K, *et al.* (2011). A SNX3-dependent retromer pathway mediates retrograde transport of the Wnt sorting receptor Wntless and is required for Wnt secretion. Nat Cell Biol 13, 914–923.

Henne WM, Buchkovich NJ, Emr SD (2011). The ESCRT pathway. Dev Cell 21, 77–91.

Hirano S, Kawasaki M, Ura H, Kato R, Raiborg C, Stenmark H, Wakatsuki S (2006). Double-sided ubiquitin binding of Hrs-UIM in endosomal protein sorting. Nat Struct Mol Biol 13, 272–277.

Hodge CD, Spyracopoulos L, Glover JN (2016). Ubc13: the Lys63 ubiquitin chain building machine. Oncotarget 7, 64471–64504.

Huang F, Zeng X, Kim W, Balasubramani M, Fortian A, Gygi SP, Yates NA, Sorkin A (2013). Lysine 63-linked polyubiquitination is required for EGF receptor degradation. Proc Natl Acad Sci USA 110, 15722–15727.

Kvainickas A, Jimenez-Orgaz A, Nagele H, Hu Z, Dengjel J, Steinberg F (2017). Cargo-selective SNX-BAR proteins mediate retromer trimer independent retrograde transport. J Cell Biol, DOI:10.1083/jcb.201702137.

Lauvrak SU, Torgersen ML, Sandvig K (2004). Efficient endosome-to-Golgi transport of Shiga toxin is dependent on dynamin and clathrin. J Cell Sci 117, 2321–2331.

Lauwers E, Erpapazoglou Z, Haguenauer-Tsapis R, Andre B (2010). The ubiquitin code of yeast permease trafficking. Trends Cell Biol 20, 196–204.

Liu J, Li M, Li L, Chen S, Wang X (2018). Ubiquitination of the PI3-kinase VPS-34 promotes VPS-34 stability and phagosome maturation. J Cell Biol 217, 347–360.

MacDonald C, Buchkovich NJ, Stringer DK, Emr SD, Piper RC (2012). Cargo ubiquitination is essential for multivesicular body intralumenal vesicle formation. EMBO Rep 13, 331–338.

Mayers JR, Fyfe I, Schuh AL, Chapman ER, Edwardson JM, Audhya A (2011). ESCRT-0 assembles as a heterotetrameric complex on membranes and binds multiple ubiquitinylated cargoes simultaneously. J Biol Chem 286, 9636–9645.

Norris A, Tammineni P, Wang S, Gerdes J, Murr A, Kwan KY, Cai Q, Grant BD (2017). SNX-1 and RME-8 oppose the assembly of HGRS-1/ESCRT-0 degradative microdomains on endosomes. Proc Natl Acad Sci USA 114, E307–E316.

Pan CL, Baum PD, Gu M, Jorgensen EM, Clark SG, Garriga G (2008). *C. elegans* AP-2 and retromer control Wnt signaling by regulating mig-14/Wntless. Dev Cell 14, 132–139.

Pan CL, Howell JE, Clark SG, Hilliard M, Cordes S, Bargmann CI, Garriga G (2006). Multiple Wnts and frizzled receptors regulate anteriorly directed cell and growth cone migrations in *Caenorhabditis elegans*. Dev Cell 10, 367–377.

Popoff V, Mardones GA, Bai SK, Chambon V, Tenza D, Burgos PV, Shi A, Benaroch P, Urbe S, Lamaze C, *et al.* (2009). Analysis of articulation between clathrin and retromer in retrograde sorting on early endosomes. Traffic 10, 1868–1880.

Popoff V, Mardones GA, Tenza D, Rojas R, Lamaze C, Bonifacino JS, Raposo G, Johannes L (2007). The retromer complex and clathrin define an early endosomal retrograde exit site. J Cell Sci 120, 2022–2031.

Port F, Kuster M, Herr P, Furger E, Banziger C, Hausmann G, Basler K (2008). Wingless secretion promotes and requires retromer-dependent cycling of Wntless. Nat Cell Biol 10, 178–185.

Raiborg C, Bache KG, Gillooly DJ, Madshus IH, Stang E, Stenmark H (2002). Hrs sorts ubiquitinated proteins into clathrin-coated microdomains of early endosomes. Nat Cell Biol 4, 394–398.

Raiborg C, Bache KG, Mehlum A, Stang E, Stenmark H (2001a). Hrs recruits clathrin to early endosomes. EMBO J 20, 5008–5021.

Raiborg C, Bremnes B, Mehlum A, Gillooly DJ, D'Arrigo A, Stang E, Stenmark H (2001b). FYVE and coiled-coil domains determine the specific localisation of Hrs to early endosomes. J Cell Sci 114, 2255–2263.

Raiborg C, Stenmark H (2009). The ESCRT machinery in endosomal sorting of ubiquitylated membrane proteins. Nature 458, 445–452.

Raiborg C, Wesche J, Malerod L, Stenmark H (2006). Flat clathrin coats on endosomes mediate degradative protein sorting by scaffolding Hrs in dynamic microdomains. J Cell Sci 119, 2414–2424.

Ren X, Hurley JH (2010). VHS domains of ESCRT-0 cooperate in high-avidity binding to polyubiquitinated cargo. EMBO J 29, 1045–1054.

Sachse M, Urbe S, Oorschot V, Strous GJ, Klumperman J (2002). Bilayered clathrin coats on endosomal vacuoles are involved in protein sorting toward lysosomes. Mol Biol Cell 13, 1313–1328.

Saint-Pol A, Yelamos B, Amessou M, Mills IG, Dugast M, Tenza D, Schu P, Antony C, McMahon HT, Lamaze C, Johannes L (2004). Clathrin adaptor epsinR is required for retrograde sorting on early endosomal membranes. Dev Cell 6, 525–538.

Sano H, Eguez L, Teruel MN, Fukuda M, Chuang TD, Chavez JA, Lienhard GE, McGraw TE (2007). Rab10, a target of the AS160 Rab GAP, is required for insulin-stimulated translocation of GLUT4 to the adipocyte plasma membrane. Cell Metab 5, 293–303.

Sato M, Konuma R, Sato K, Tomura K, Sato K (2014). Fertilization-induced K63-linked ubiquitylation mediates clearance of maternal membrane proteins. Development 141, 1324–1331.

Seaman MN (2012). The retromer complex—endosomal protein recycling and beyond. J Cell Sci 125, 4693–4702.

Shi A, Chen CC, Banerjee R, Glodowski D, Audhya A, Rongo C, Grant BD (2010). EHBP-1 functions with RAB-10 during endocytic recycling in *Caenorhabditis elegans*. Mol Biol Cell 21, 2930–2943.

Shi A, Liu O, Koenig S, Banerjee R, Chen CC, Eimer S, Grant BD (2012). RAB-10-GTPase-mediated regulation of endosomal phosphatidylinositol-4,5-bisphosphate. Proc Natl Acad Sci USA 109, E2306–E2315.

Shi A, Sun L, Banerjee R, Tobin M, Zhang Y, Grant BD (2009). Regulation of endosomal clathrin and retromer-mediated endosome to Golgi retrograde transport by the J-domain protein RME-8. EMBO J 28, 3290–3302.

Simonetti B, Danson CM, Heesom KJ, Cullen PJ (2017). Sequence-dependent cargo recognition by SNX-BARs mediates retromer-independent transport of CI-MPR. J Cell Biol 216, 3695–3712.

Sulston JE, Horvitz HR (1977). Post-embryonic cell lineages of the nematode, *Caenorhabditis elegans*. Dev Biol 56, 110–156.

Tanno H, Komada M (2013). The ubiquitin code and its decoding machinery in the endocytic pathway. J Biochem 153, 497–504.

Yang PT, Lorenowicz MJ, Silhankova M, Coudreuse DY, Betist MC, Korswagen HC (2008). Wnt signaling requires retromer-dependent recycling of MIG-14/Wntless in Wnt-producing cells. Dev Cell 14, 140–147.